SEC-10 and RAB-10 coordinate basolateral recycling of clathrin-independent cargo through endosomal tubules in *Caenorhabditis elegans*

Sanyou Chen[a,1], Lei Li[a,1], Jiangli Li[a,1], Bei Liu[a], Xinyu Zhu[a], Li Zheng[b], Rongying Zhang[a,2], and Tao Xu[a,b,2]

[a]Key Laboratory of Molecular Biophysics of the Ministry of Education, College of Life Science and Technology, Huazhong University of Science and Technology, Wuhan, Hubei 430074, China; and [b]National Laboratory of Biomacromolecules, Institute of Biophysics, Chinese Academy of Sciences, Beijing 100101, China

Edited by Thomas C. Südhof, Stanford University School of Medicine, Stanford, CA, and approved September 15, 2014 (received for review May 6, 2014)

Despite the increasing number of regulatory proteins identified in clathrin-independent endocytic (CIE) pathways, our understanding of the exact functions of these proteins and the sequential manner in which they function remains limited. In this study, using the *Caenorhabditis elegans* intestine as a model, we observed a unique structure of interconnected endosomal tubules, which is required for the basolateral recycling of several CIE cargoes including hTAC, GLUT1, and DAF-4. SEC-10 is a subunit of the octameric protein complex exocyst. Depleting SEC-10 and several other exocyst components disrupted the endosomal tubules into various ring-like structures. An epistasis analysis further suggested that SEC-10 operates at the intermediate step between early endosomes and recycling endosomes. The endosomal tubules were also sensitive to inactivation of the Rab GTPase RAB-10 and disruption of microtubules. Taken together, our data suggest that SEC-10 coordinates with RAB-10 and microtubules to form the endosomal tubular network for efficient recycling of particular CIE cargoes.

endosomal tubules | recycling | microtubule | clathrin-independent endocytosis | live worm imaging

There has been increased interest in clathrin-independent endocytic (CIE) pathways over the past 10 y, and a growing list of endogenous plasma membrane (PM) proteins that enter cells by CIE pathways has been identified (1–3). Many CIE cargo proteins, such as the major histocompatibility complex class I (MHCI), the α-chain of the IL-2 receptor (TAC), CD59, CD44, and CD147, have been confirmed to follow the Arf6-associated CIE pathway, which is highly conserved from *Caenorhabditis elegans* to mammalian cells (3). Several players, including Rab10, Rab22, Rab35, Hook1, ALX-1, and RME-1/EHD-1, have been identified to modulate the recycling of CIE cargoes through different itineraries (3–8).

Notably, CIE is under differential regulation on the apical and basolateral poles of polarized cells, and evidence points to a larger fraction of CIE on the basolateral pole of MDCK cells (9). Human TAC (hTAC) has been used to study canonical CIE pathway in the *C. elegans* intestine, which is an attractive model system for studying polarized intracellular trafficking (6, 10). Interestingly, a rapid basolateral recycling pathway has been revealed and several factors involved in the recycling of CIE cargoes have been identified, such as RAB-10, RME-1/EHD-1, ALX-1, and EHBP-1 (6–8, 11). However, it remains unclear how these proteins coordinate and regulate the trafficking of CIE cargoes through different endosomal intermediates.

The exocyst is an evolutionarily conserved octameric complex composed of Sec3, Sec5, Sec6, Sec8, Sec10, Sec15, Exo70, and Exo84 (12, 13). This complex was originally proposed to function in post-Golgi secretion/exocytosis by tethering exocytic vesicles with the PM (12–14). Consistent with this idea, the exocyst localizes to the PM where exocytosis actively occurs and has been implicated in many cellular trafficking processes including polarized budding in yeast (14), neurite growth in neurons (15), GLUT4 membrane insertion in fat cells (16), and cell migration (17–19). Recent studies have revealed an association between the exocyst and recycling endosome-localized proteins, such as Arf6 (20), AP1B (21), and Rab11 (22), and the presence of exocyst on multiple populations of endosomes (23). Interfering with exocyst functions affects several endocytic pathways, such as transferrin receptor (TfR) recycling in nonpolarized cells (20), and apical and basolateral recycling in polarized cells (23, 24). However, the mechanisms of how the exocyst participates in membrane recycling remain poorly understood. Attempts to examine the exact function of the exocyst in higher organisms using gene knockout methods have not been fruitful because exocyst mutations lead to embryo or larval lethality both in *Drosophila* and mice (25–27).

Taking advantage of the powerful genetic tools available for *C. elegans*, we previously isolated a novel *sec-10* C-terminal truncated mutation (28). The homozygous mutant is sterile but survives to adulthood. Here, using high-resolution live imaging of the *C. elegans* intestine, we show that *sec-10* mutants display defects in basolateral recycling of particular CIE cargoes. We identified an extensive network of endosomal tubules used for efficient basolateral recycling. We propose that the concerted action of SEC-10, RAB-10, and microtubules is required to form interconnected endosomal tubules.

Significance

Understanding how clathrin-independent endocytic (CIE) cargo proteins are sorted into and transported within endosomes has attracted growing interests. Here, in *Caenorhabditis elegans* intestine, a well-established genetic system for deciphering endocytic trafficking in multicellular organisms, we report direct visualization of dynamic endosomal tubules as carriers for basolateral recycling of certain CIE cargoes. We unveil the coordination of the Rab GTPase RAB-10, the exocyst component SEC-10, and the microtubule cytoskeleton to form a network of interconnected tubules. We demonstrate that RAB-10 leads the growing tubules and that SEC-10 is required for tethering/fusion of tubular carriers. Our results provide previously unidentified insights into the regulation of CIE pathways.

Author contributions: R.Z. and T.X. designed research; S.C., L.L., J.L., X.Z., and L.Z. performed research; B.L. contributed new reagents/analytic tools; S.C., L.L., and J.L. analyzed data; and R.Z. and T.X. wrote the paper.

The authors declare no conflict of interest.

This article is a PNAS Direct Submission.

Freely available online through the PNAS open access option.

[1]S.C., L.L., and J.L. contributed equally to this work.

[2]To whom correspondence may be addressed. Email: xutao@ibp.ac.cn or ryzhang@mail.hust.edu.cn.

This article contains supporting information online at www.pnas.org/lookup/suppl/doi:10.1073/pnas.1408327111/-/DCSupplemental.

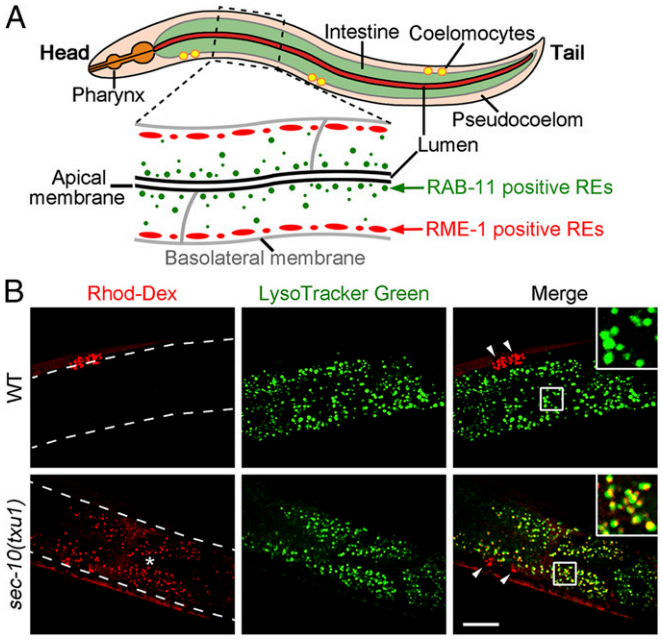

Fig. 1. Mutation in *sec-10* causes missorting of basolaterally uptaked fluid cargoes into LROs in the *C. elegans* intestine. (*A*) Illustration showing the arrangement of the intestine. The basolateral and apical membranes of the intestine are indicated. RME-1– and RAB-11–labeled REs align along the basolateral and apical membrane, respectively. (*B*) Rhod-Dex was injected into the pseudocoeloms of animals that were prestained with LysoTracker Green to label intestinal LROs. Images were taken 1 h after injection. After injection, Rhod-Dex will follow the fast basolateral recycling pathway: Be endocytosed via the CIE pathway, pass through RAB-5–postive early endosome and RME-1–positive recycling endosome, be efficiently recycled out of the intestines, and finally be uptaked by the pseudocoelom scavenger cells, coelomocytes. Hence, no Rhod-Dex signal will be observed in the intestine of WT animals. If this fast basolateral recycling pathway is blocked, i.e., in *sec-10* mutants, Rhod-Dex will be accumulated in the intestine and be missorted into LysoTracker-stained LROs. Asterisk depicts the lumen of the intestine. Arrowheads point to coelomocytes with internalized Rhod-Dex. The contours of intestines are outlined in red channels. (Scale bar: 20 μm.)

Results

The Exocyst Is Required for Basolateral Recycling in the *C. elegans* Intestine. To address the function of the exocyst, we previously generated a deletion mutant of the exocyst component *sec-10(txu1)* in *C. elegans* (Fig. S1*A*) (28). The transcriptional expression profile of *sec-10* was ubiquitous (Fig. S1*B*) (28), in agreement with other exocyst subunits such as *sec-5* (29), *exoc-7*, and *sec-6* (30).

The worm intestine is a highly polarized epithelial tube with the apical microvillar surface facing the lumen and the basolateral surface facing the pseudocoelom (body cavity), where three pairs of coelomocytes are located (Fig. 1*A*). To test the involvement of exocyst in postendocytic intracellular trafficking, we used the well-established in vivo endocytic assay in the *C. elegans* intestine (7). Internalization of the fluid-phase marker rhodamine-dextran (Rhod-Dex) or lipophilic dye FM4-64 from the apical side was not different in *sec-10* mutants from that in wild-type (WT) N2 worms, and both markers reached the so-called gut granules (Fig. S2 *A* and *B*). Gut granules are lysosome-related organelles (LROs) that can be identically identified by both autofluorescence and the lysosome marker, LysoTracker (31, 32). In contrast, the fast recycling of basolaterally applied Rhod-Dex was blocked in *sec-10* mutants and accumulated in LROs, whereas lysosome-destined FM4-64 was not affected (Fig. 1*B* and Fig. S2 *C* and *D*). A similar blockade of fluid-phase marker recycling was observed in the absence of SEC-5, another component of the exocyst complex (Fig. S2 *E* and *F*). These data indicate that the SEC-10 and SEC-5 exocyst components are specifically involved in the basolateral recycling of internalized fluid-phase cargoes.

Dual Involvement of SEC-10 in Apical and Basolateral Endosomal Recycling in the *C. elegans* Intestine. A previous study on MDCK cells suggested that the exocyst, through its Sec15 component, may function as a Rab11 effector to regulate basolateral-to-apical transcytosis (23). The *sec15* mutant in the *fly* photoreceptor results in strong accumulation of Rab11 within the apical membranes of the photoreceptor (22). We confirmed the accumulation of RAB-11–positive vesicles at the apical PM in *sec-10* mutants (Fig. 2 *A* and *B*) or after *sec-15* RNAi knockdown (Fig. S3 *A* and *B*) (10). The accumulation was caused by unsuccessful tethering or fusion of RAB-11–positive vesicles with the PM (Fig. 2*C* and Movie S1) in the absence of SEC-10.

Next, we sought to dissect the role of the exocyst in basolateral recycling. Using a 150× oil objective lens, we observed the enrichment of RME-1, which labels basolateral recycling endosomes (BREs) (7, 33), in unique tubulovesicular arrays immediately underneath the basolateral PM and to a much lesser extent in the subapical domains (Fig. 2*D*) (6). However, the morphology of the RME-1–positive structures was altered from extensive tubulovesicular structures to isolated puncta at the basolateral

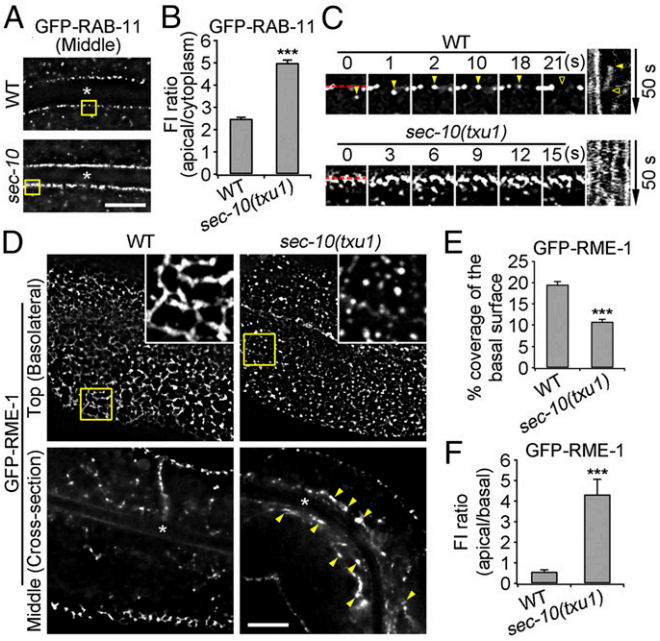

Fig. 2. The apical and basolateral recycling endosomal systems were differentially affected in *sec-10* mutants. (*A*) Micrographs of intestinal GFP-RAB-11 in WT and *sec-10* mutant worms. (*B*) The average fluorescence intensity (FI) ratio of apical PM-associated RAB-11 signals relative to cytoplasma signals. n = 142/125 areas from 40/41 animals (WT/*sec-10*). ***$P < 0.001$ (Student's t test). (*C*) Individual mobile RAB-11 vesicles approaching the apical PM in WT and *sec-10* animals. Arrowheads in the tile view indicating a translocating event from the cytoplasm to the apical PM. (*C, Right*) Kymograph of the red dash lines indicated in *C, Left*. (*D*) GFP-RME-1–labeled basolateral structures in WT and *sec-10*. Arrowheads indicate the aberrant increase of GFP-RME-1 on the apical domain. Asterisks depict the lumen of the intestine. (*E*) Coverage percentage of the basolateral surface by GFP-RME-1, as the magnified regions shown in *D*, was quantified. n = 28/20 areas from 14/10 animals (WT/*sec-10*). ***$P < 0.001$ (Student's t test). (*F*) FI ratio of GFP-RME-1 between apical and basal side. A 20-pixel-wide and a 10-pixel-wide region along apical and basal PM, as shown in *D, Lower*, were selected for the quantification. n = 49/36 areas from 20/14 animals (WT/*sec-10*). ***$P < 0.001$ (Mann–Whitney rank sum test). Error bars represent SEM. (Scale bars: 10 μm.)

CELL BIOLOGY

side in *sec-10* mutants, with shrinkage of approximately one-half of the occupied area (Fig. 2 *D* and *E*). In contrast, the number of RAB-5–positive early endosomes and RAB-7–positive late endosomes was increased (Fig. S3 *C–G*), along with the RME-1 intensity at the apical side (Fig. 2 *D* and *F*), in *sec-10* mutants. Thus, *sec-10* mutation seems to block basolateral recycling at a step upstream of BRE, which causes partial redistribution of RME-1 to the apical side. Our data suggest that SEC-10 plays different roles in apical and basolateral recycling, including the accumulation of RAB-11–positive vesicles on the apical side, while reducing RME-1–positive structures on the basolateral side. A similar reduction of BRE was observed by depleting SEC-15 (Fig. S3 *H–J*).

SEC-10 Regulates Basolateral Recycling in a Cargo-Specific Manner. Next, to understand how the exocyst acts in the basolateral recycling pathway, we explored the intermediate transporting structures of two typical recycling cargo proteins: hTAC, an Arf6-dependent CIE cargo, and hTfR (human transferrin receptor), a classical clathrin-dependent endocytic (CDE) cargo (34).

Under low magnification imaging (60× objective), prominent localization of hTAC-GFP was observed with intracellular signals along the basolateral PM (6), which decreased by ∼60% in *sec-10* mutants (Fig. 3 *A* and *J*). Under high resolution (150× objective) imaging, most of the subplasmalemmal hTAC-GFPs existed in a delicate tubular network (Fig. 3*B*). To confirm the endosomal identity of this tubular network, the mCherry-TRAM transgene, which labels the endosomal reticulum (ER) (35, 36), was introduced into hTAC-GFP transgenic worms (Fig. S4). The ER tubular network was distributed both underneath the PM (top layer) and to the deeper cytosol (middle layer), whereas the hTAC tubular network was enriched underneath the basolateral PM (Fig. S4*A*). The diameter of ER tubules was approximately two times that of the hTAC-positive tubules (Fig. S4*B*). A linear profile analysis revealed no overlapping between these two tubular networks (Fig. S4 *C* and *D*). Mutation in *sec-10* had no effect on either the morphology or intensity of mCherry-TRAM (Fig. S4 *E* and *F*). Therefore, the majority of subplasmalemmal hTAC-positive tubules were endosomal, and not ER derived.

Live imaging of intestinal hTAC-GFP showed that a small portion of these endosomal tubules were dynamic, with tubules extending and fusing into adjacent structures (Fig. 3*C* and Movie S2), which has not been observed before (6, 11, 37, 38). Strikingly, the delicate tubular network collapsed in *sec-10* mutants, with a concomitant increase in various ring-like structures (Fig. 3 *B* and *D–G* and Movie S3). This phenotype was fully rescued by the transgenic expression of T7-tagged SEC-10 (Fig. S5 *A* and *B*). More than 70% of the hTAC tubular structures were fragmented (Fig. 3*G*), whereas the number of ring-like structures increased by approximately sixfold in *sec-10* mutants (Fig. 3*F*). A similar disruption of the hTAC-positive tubular network was demonstrated following RNAi treatment of seven of eight exocyst components (Fig. S5 *C–E*). In contrast, no detectable differences in the number, distribution, or morphology of the hTfR-GFP–containing vesicular structures (6) were observed in *sec-10* mutants (Fig. 3 *H*, *I*, and *K*).

The finding that hTAC and hTfR are localized largely on tubular and vesicular structures, respectively, is reminiscent of recent progress in cultured mammalian cells (39). It is also consistent with notions that the pleiomorphic and tubular carriers account for the entry and trafficking of many cargo proteins following different CIE pathways (3, 5, 40). To verify the generality of our finding, we further examined two other endogenous CIE cargo proteins: GLUT1 and DAF-4 (dauer formation-defective-4), the *C. elegans* homolog of type II BMP (bone morphogenetic protein) receptor. Both proteins are CIE cargoes that are transported via the Arf6-associated itinerary (2, 35, 41). As shown in Fig. S6*A*, *C. elegans* GLUT1 colocalized perfectly with hTAC in tubular structures. The subplasmalemmal tubular structures of GLUT1 and DAF-4 were similarly fragmented in *sec-10* mutants (Fig. S6 *B* and *C*) as hTAC-positive tubular structures. As a comparison, localization of MIG-14, another endogenous CDE cargo (42–44), was confined to vesicular structures and was not altered in *sec-10* mutants (Fig. S6 *B* and *D*).

SEC-10 Is Specifically Involved in Intermediate Step(s) in the Basolateral Recycling Pathway. Next we elucidated the step at which SEC-10 acts in the basolateral recycling pathway. Most of the subplasmalemmal hTAC tubular structures colocalized with RME-1–labeled BREs

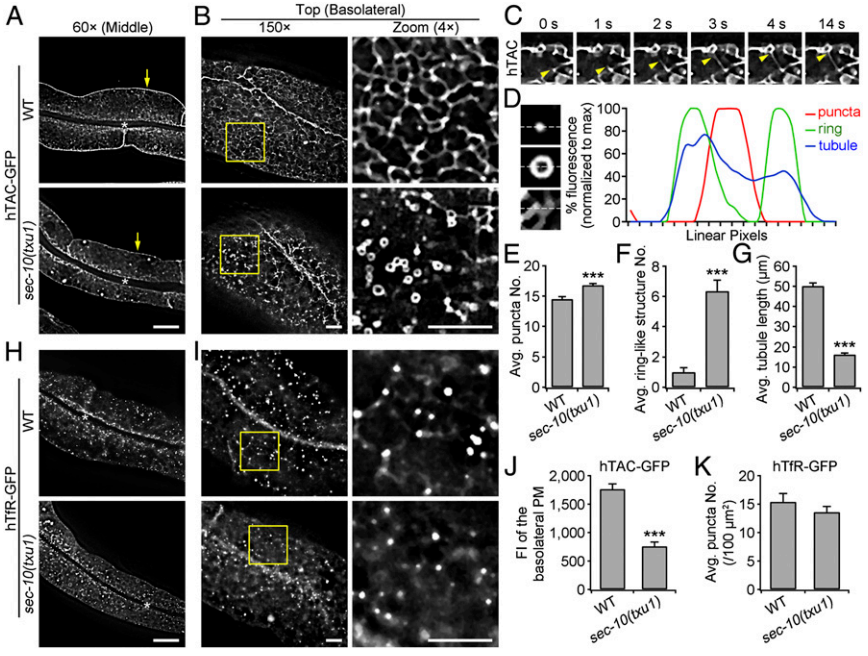

Fig. 3. The distribution and patterns of hTAC-containing endosomal structures are altered in *sec-10* mutants. (*A* and *H*) Micrographs magnified at 60× show loss of basolateral PM-associated hTAC-GFP (*A*) and no detectable difference for the endosomal localization of hTfR-GFP in *sec-10* (*H*). Arrows in *A* indicate basolateral PM-associated hTAC. (*B* and *I*) Micrographs magnified at 150× provide detailed architectures for hTAC (*B*) and hTfR (*I*) signal. (*C*) A live worm imaging of the WT intestine shows a dynamic hTAC-containing tubule. Arrowheads mark the extending tip of a tubule. (*D–G*) Profiles of the hTAC-containing transport intermediates in *sec-10* (*D*). The number of puncta (*E*), ring-like structures (*F*), and the length of tubules (*G*) per 100 μm^2 were calculated for WT and *sec-10* worms. n = 37/103 areas from 25/45 animals (WT/*sec-10*). ***$P < 0.001$, puncta and tubule (Student's t test), ring-like structure (Mann–Whitney rank sum test). (*J*) Average FI of hTAC per unit length along the basolateral PM in *A*. (*K*) Quantification of the number of hTfR-containing puncta in *I*. n = 10 animals for each group in *J* and *K*. ***$P < 0.001$ (Student's t test). Error bars represent SEM. (Scale bars: *A* and *H*, 20 μm; *B* and *I*, 5 μm.)

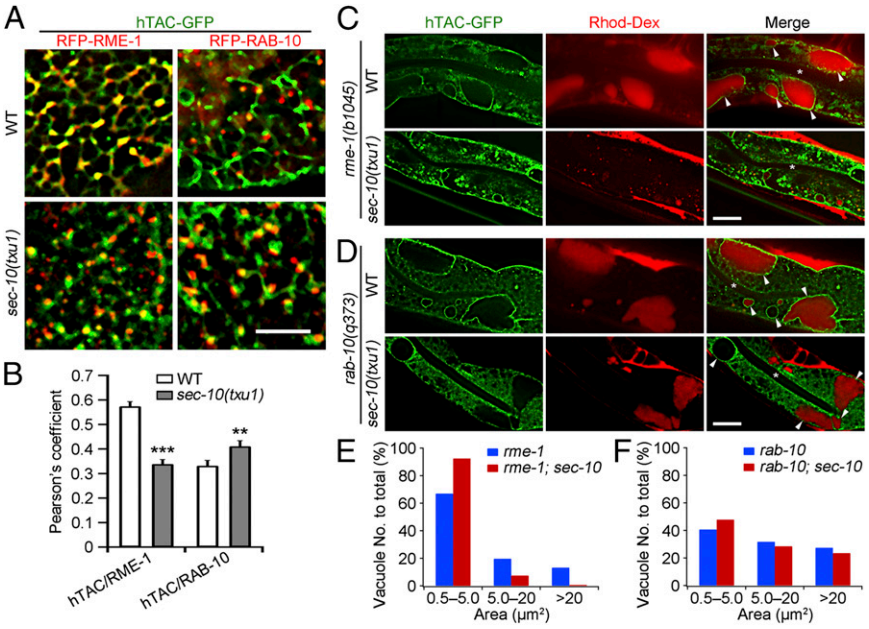

Fig. 4. SEC-10 functions between BEEs and BREs during basolateral recycling. (*A*) Colocalization images of hTAC-GFP with RFP-RME-1 or RFP-RAB-10 in WT and *sec-10* mutant intestines. (*B*) Quantification of the colocalization by Pearson's colocalization coefficient. RFP-RME-1 group, $n = 18/19$ areas from seven animals (WT/*sec-10*), $^{***}P < 0.001$; RFP-RAB-10 group, $n = 16/21$ areas from seven animals (WT/*sec-10*), $^{**}P = 0.002$, Student's *t* test. Error bars represent SEM. (*C* and *D*) Confocal images of basolaterally internalized Rhod-Dex in hTAC-GFP-expressing intestines of various mutants as indicated. Arrowheads mark endosomes larger than 20 μm^2, asterisks depict the lumen of the intestine. (*E*) Quantification of hTAC-GFP-accumulated vacuole size in *rme-1* single (688 vacuoles from 31 animals) and *rme-1; sec-10* double mutants (284 vacuoles from 24 animals). (*F*) Quantification of hTAC-GFP–accumulated vacuole size in *rab-10* single (542 vacuoles from 25 animals) and *rab-10; sec-10* double mutants (280 vacuoles from 30 animals). (Scale bars: *A*, 5 μm; *C* and *D*, 20 μm.)

with a Pearson's correlation coefficient (45) of 0.57, suggesting the recycling of hTAC *en route* through BRE (Fig. 4 *A* and *B*). The coefficient decreased to 0.33 in *sec-10* mutants, implying less colocalization of hTAC with BREs (Fig. 4*B*). RAB-10 is required at an early step in the basolateral recycling pathway upstream of RME-1 (6). RFP-RAB-10 displayed punctate distribution and was localized mostly to the tip or the junction of hTAC tubules (Figs. 4*A* and 5 *A* and *B*). The Pearson's coefficient between RAB-10 and hTAC increased slightly from 0.32 in WT to 0.40 in *sec-10* mutant intestines (Fig. 4*B*).

We then took another approach to determine the endocytic step controlled by the exocyst by generating *rme-1(b1045); sec-10(txu1)* double mutants. Consistent with a previous study (7), we verified that *rme-1* single mutants generated enlarged vacuoles of BRE origin (Fig. 4*C, Upper* and Fig. S7*B*) caused by the blockade of transport out of BRE to PM. The *sec-10* mutation largely prevented BRE vacuolation observed in *rme-1* mutants (Fig. 4*C*). Large intestinal vacuoles (approximately >20 μm^2) almost diminished in *rme-1; sec-10* double mutants (Fig. 4*E*), and the influx of Rhod-Dex into vacuoles was also substantially reduced (Fig. 4*C*; integrated Rhod-Dex intensity dropped by 62% in *rme-1; sec-10* double mutants). This result suggests that SEC-10 possibly acts upstream of RME-1 to control the influx of cargo to BRE.

A single mutation in *rab-10* also generated enlarged vacuoles (Fig. 4*D, Upper*) of early endosome origin (Fig. S7*A*) by blocking export from the basolateral early endosomes (BEEs) (6, 11). However, BEE vacuolation and trapping of Rhod-Dex in the *rab-10* vacuoles were not prevented by *sec-10* in *rab-10(q373); sec-10(txu1)* double mutants (Fig. 4 *D* and *F*), suggesting a role for SEC-10 downstream of RAB-10. Taken together, the epistasis analysis suggested that SEC-10 regulates intermediate step(s) in the basolateral recycling pathway between BEE and BRE, rather than at the PM, as observed for the apical side.

RAB-10 and SEC-10 Coordinate the Extension and Tethering of hTAC-Positive Tubules. Although RAB-10 has been implicated in basolateral recycling, the carrier it regulates remains unresolved. Using time-lapse imaging of the live-worm intestine, we found that RAB-10 was located at most (~90%) tips of the hTAC-GFP tubules (Fig. 5*A*). In particular, RAB-10 was located at the tips of newly budding tubules, during the extension process, and until the final fusion with adjacent tubules (Fig. 5*B* and Movie S4). Moreover, a constitutively active RAB-10 mutant (GTP-locked Q68L mutation) generated more extensive networks of hTAC-GFP tubules and displayed strong punctate labeling at the tubule tips (Fig. 5 *A* and *C*). In contrast, a dominant negative RAB-10 mutant (GDP-locked T23N mutation) diffused in the cytoplasm and caused large vacuoles delimited with hTAC-GFP (Fig. 5*A*), a phenotype similar to that in *rab-10* mutants (Fig. 4*D*) (6). Hardly any hTAC-positive tubules were observed in the *rab-10* mutant or the RAB-10(T23N) transgene (Figs. 4*D* and 5*A*), suggesting an essential role for RAB-10 GTPase in the budding and generation of tubules from BEEs.

In contrast to the minimal tubule extension in *rab-10* mutants, we observed remnant tubule extension at a significantly reduced rate in *sec-10* mutants compared with that in WT animals (mean 1.5 vs. 8.8 events per 100 μm^2 per 10 min, respectively) (Fig. 5 *D* and *E*). However, we noticed that the ratio of successful tethering/fusion decreased by approximately fivefold in the remnant extended tubules in *sec-10* mutants, although RAB-10 was still located at the leading tip (Fig. 5 *D* and *F* and Movie S5).

We verified by immunofluorescence microscopy that endogenous SEC-15, a vesicle-associated component of the exocyst (22, 46), partially colocalized with hTAC tubules at the branching point or at/near the end of a tubule (Fig. S8*A*). However, SEC-15 in *rab-10 (dx2)* mutants accumulated prominently around large BEE vacuoles (Fig. S8*B*), suggesting the association of certain exocyst components with the endosomal membrane even in the absence of RAB-10.

The Generation of hTAC-Positive Tubules Requires Microtubule Cytoskeletons. Accumulating evidence suggests that cytoskeletons have profound roles guiding and segregating membrane trafficking intermediates (5, 47–49). To further unravel the machinery underlying the dynamic hTAC tubules, we tested their dependence on the cytoskeleton. Nocodazole (Noc) was injected into the body cavity to acutely depolymerize the intestinal microtubules. This treatment abrogated the hTAC-positive tubular network in a manner similar to the *sec-10* mutation, causing tubule fragmentation (Fig. S9 *A* and *B*). In contrast, neither latrunculin B (LatB) treatment, which disrupts actin filaments, nor knockdown of actin by RNAi altered the hTAC-positive tubules (Fig. S9 *A–C* and Movie S6). The density and patterns of hTfR-containing vesicular structures were not altered in worms treated with either Noc or LatB (Fig. S9*D*).

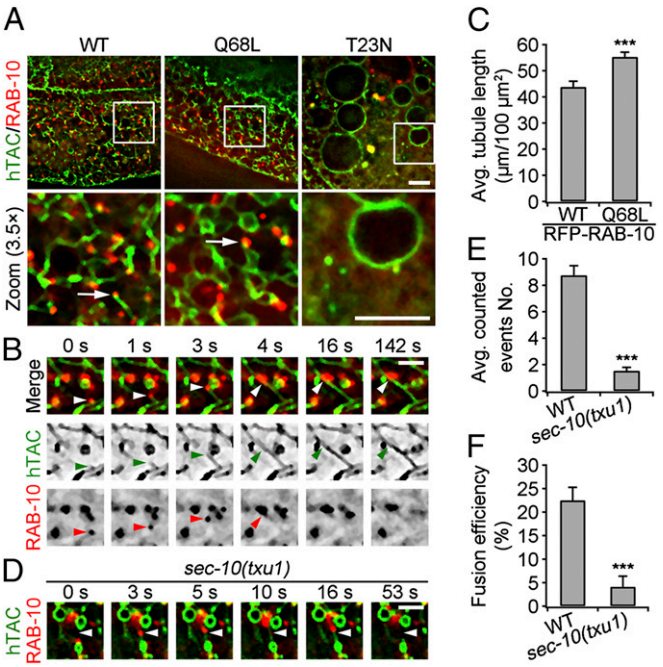

Fig. 5. SEC-10 regulates the tethering/fusion of RAB-10–guided hTAC tubules. (*A*) The *C. elegans* intestine coexpressing RFP-tagged WT, Q68L, or T23N mutant RAB-10 and hTAC-GFP were imaged by confocal fluorescence microscopy, respectively. Note the decoration of RAB-10 on the tip or junction of hTAC tubular network (arrows). (*B*) Live worm imaging of the transgenic animals coexpressing hTAC-GFP and mRFP-RAB-10. A series of frames are shown depicting the generation and extension of a hTAC-containing tubule (green) that is guided by the RAB-10 (red) at the leading edge and the tethering/fusion of the newly growing tubule to an adjacent tubule. Arrowheads mark the dynamic events. (*C*) The average length of hTAC-positive tubules, in RFP-RAB-10 WT and Q68L mutant background, was calculated. n = 14/16 areas from 11/8 animals (WT/*sec-10*). ***$P < 0.001$ (Mann–Whitney rank sum test). (*D*) As in *B* from a *sec-10* mutant worm. Arrowheads mark a dynamic event depicting the unsuccessful fusion of a newly growing hTAC tubule. (*E*) Quantification of the number of hTAC-positive tubule extension events as in *B* and *D* that occurred in a 100-μm^2 square over a 10-min time course. (*F*) Fusion efficiency was calculated to divide the number of successful fusion events by the number of total extension events as in *E*. n = 31/35 regions (WT/*sec-10*), 20 animals for each group. ***$P < 0.001$ (Mann–Whitney rank sum test). Error bars represent SEM. (Scale bars: *A*, 5 μm; *B* and *D*, 2 μm.)

Discussion

Ultrastructural studies have identified morphologically distinct pleiomorphic and tubular carriers for both entry and trafficking of CIE cargo proteins (5, 40). Endosomal tubules, with a high ratio of membrane surface to luminal volume, afford an effective way to concentrate recycling cargoes and ensure efficient transport of CIE cargoes within endosomes (3–5). However, it remains a challenge to delineate how these tubules are generated and regulated. In the current study, we discovered in the intact *C. elegans* intestine using high magnification (150×) live worm confocal imaging that several Arf6-dependent CIE cargoes (hTAC, GLUT1, and DAF-4) reside on basolateral endosomal tubules. The current model proposes that cargo sorted into tubules will undergo vesiculation and fission, allowing the formation of transport vesicles that move along microtubules and return to the cell surface (50). However, we failed to observe fission and vesiculation of extending tubules following the extension of hTAC tubules. These newly formed tubules rather fused with adjacent tubular carriers (Figs. 3*C* and 5*B*) or BREs to form an extensive network that bridged between BEE and BRE. We verified that the tubular network observed here was not ER (Fig. S4). It remains to be tested whether this tubular network is exclusive to polarized intestine in *C. elegans* or it also exists in mammalian cells. It should be noted that this itinerary may only be followed by a subset of CIE cargoes due to the existence of different CIE trafficking pathways (3).

Formation of this tubular network clearly requires coordination of protein machinery at various stages during membrane budding, extension, and tethering/fusion of the tubules. In this study, we identified three players, including RAB-10, exocyst, and cytoskeleton microtubules that are required to form the basolateral recycling tubular network. Although RAB-10 is implicated in controlling the exit of cargo from EE (Fig. S7*A*) (6, 51), it is unclear as to which exiting carriers are regulated by RAB-10 and how they operate. Here, we demonstrated that RAB-10 was localized at the "leading edge" of the dynamic hTAC tubules and predicted the path where the growing tubules would travel (Fig. 5*B*). Inactivating RAB-10 nearly completely abolished the tubule extensions and gave rise to giant EE vacuoles (Figs. 4*D* and 5*A* and Fig. S7*A*). A similar leading function has been proposed for Rab10 in ER dynamic tubules of COS-7 cells (52). Considering the broad subcellular distribution of Rab10 GTPase, it is not surprising that Rab10 may be a versatile membrane transportation regulator in different cellular contexts (6, 52–54).

The canonical function of the exocyst complex is thought to tether exocytic or recycling vesicles to the PM for subsequent fusion (23, 55). Here, we demonstrated that SEC-10 tethered the apical recycling vesicles to the PM, which is not the case for basolateral postendocytic trafficking. In the absence of SEC-10, the basolateral endosomal tubules were largely fragmented into small ring-like structures (Fig. 3*B*). This phenotype is different from the complete disappearance of hTAC-positive tubules and the appearance of giant vacuoles in *rab-10* mutants, suggesting different involvement of RAB-10 and SEC-10 in generating endosomal tubules. Our epistasis analysis placed the SEC-10 action site between RAB-10 and RME-1 (Fig. 4). We also demonstrated increased failure of tethering/fusion between hTAC-positive tubules caused by the *sec-10* mutation (Fig. 5 *D* and *F*). Thus, it is likely that SEC-10 functions to stabilize the growing tubule by tethering it to other tubules, thereby forming a tubular network structure. Without stable tethering, the growing tubule is prone to fragmentation by a RAB-10–mediated pulling force. This SEC-10 function is reminiscent of the Hook1 tethering protein (5), which specifically participates in sorting of other CIE cargoes that directly recycle from the sorting endosomes back to the PM. RNAi knockdown seven out of the eight exocyst components resulted in similar disruption of hTAC-positive endosomal tubules (Fig. S5 *D* and *E*), suggesting that the tethering function is likely carried out by most of the exocyst components.

Our results also revealed that microtubules are required to stabilize the hTAC tubules, suggesting the importance of the microtubule cytoskeleton in the formation of basolateral endosomal tubules (Fig. S9). The pulling force during the generation of hTAC tubules is likely mediated by RAB-10 through a motor protein moving along the microtubules. Rab proteins allow the directional movement of various membrane carriers along the microtubule cytoskeleton through a direct or indirect association with motor proteins (56). In addition, a connection of the exocyst as adaptors with microtubules and actin-based transport has been suggested (15, 57–59).

Collectively, our data propose a model of sequential actions: RAB-10 functions in the budding of membrane tubules and provides the pulling force for extension along the microtubules. Subsequently, the exocyst complex mediates tethering/fusion of endosomal tubules to form a stable tubular network. However, alternatives should also be considered, i.e., the exocyst could work together with RAB-10 during the budding and extension of endosomal tubules. Indeed, numerous proteins have been identified to interact with the exocyst, and it has been assumed that the exocyst is involved in multiple trafficking stages (55, 60).

Although no direct interaction was detected between RAB-10 and exocyst by the yeast two-hybrid assay or coimmunoprecipitation (Fig. S8 *C–E*), transient or indirect interactions cannot be excluded. The less severe phenotype of the *sec-10* mutant could also be explained by incomplete loss of function of the exocyst complex in the absence of SEC-10. Future studies will be required to determine exactly how RAB-10, the exocyst, molecular motors, and microtubules coordinate to construct the tubular network during basolateral recycling of CIE cargoes.

Materials and Methods

Full methods, including plasmid and transgenic strain construction, yeast two-hybrid assay, immunostaining and endocytosis assay in intestines, coimmunoprecipitation analysis, RNA interference, quantitative PCR analysis, microscopy, image analysis, Pearson's colocalization coefficient, and statistical analysis are found in *SI Materials and Methods*.

General Methods and Strains. All *C. elegans* strains were derived originally from the wild-type Bristol strain N2. Worm cultures, genetic crosses, and other strain manipulation methods were essentially those described by Brenner (61). A complete list of strains used in this study can be found in Table S1.

ACKNOWLEDGMENTS. We thank Barth Grant, Erik Jorgensen, and Xiaochen Wang for providing strains and plasmids, and we are especially grateful to Dr. A. Shi for critical reading and comments on the manuscript. This work was supported by Major State Basic Research Program of China Grants 2011CB910400 and 2010CB833701 and National Science Foundation of China Grant 31071249.

1. Radhakrishna H, Donaldson JG (1997) ADP-ribosylation factor 6 regulates a novel plasma membrane recycling pathway. *J Cell Biol* 139(1):49–61.
2. Eyster CA, et al. (2009) Discovery of new cargo proteins that enter cells through clathrin-independent endocytosis. *Traffic* 10(5):590–599.
3. Maldonado-Báez L, Williamson C, Donaldson JG (2013) Clathrin-independent endocytosis: A cargo-centric view. *Exp Cell Res* 319(18):2759–2769.
4. Weigert R, Yeung AC, Li J, Donaldson JG (2004) Rab22a regulates the recycling of membrane proteins internalized independently of clathrin. *Mol Biol Cell* 15(8):3758–3770.
5. Maldonado-Báez L, Cole NB, Krämer H, Donaldson JG (2013) Microtubule-dependent endosomal sorting of clathrin-independent cargo by Hook1. *J Cell Biol* 201(2):233–247.
6. Chen CC, et al. (2006) RAB-10 is required for endocytic recycling in the *Caenorhabditis elegans* intestine. *Mol Biol Cell* 17(3):1286–1297.
7. Grant B, et al. (2001) Evidence that RME-1, a conserved *C. elegans* EH-domain protein, functions in endocytic recycling. *Nat Cell Biol* 3(6):573–579.
8. Shi A, et al. (2007) A novel requirement for *C. elegans* Alix/ALX-1 in RME-1-mediated membrane transport. *Curr Biol* 17(22):1913–1924.
9. Sandvig K, van Deurs B (2005) Delivery into cells: Lessons learned from plant and bacterial toxins. *Gene Ther* 12(11):865–872.
10. Winter JF, et al. (2012) *Caenorhabditis elegans* screen reveals role of PAR-5 in RAB-11-recycling endosome positioning and apicobasal cell polarity. *Nat Cell Biol* 14(7):666–676.
11. Shi A, et al. (2010) EHBP-1 functions with RAB-10 during endocytic recycling in *Caenorhabditis elegans*. *Mol Biol Cell* 21(16):2930–2943.
12. Hsu SC, et al. (1996) The mammalian brain rsec6/8 complex. *Neuron* 17(6):1209–1219.
13. TerBush DR, Maurice T, Roth D, Novick P (1996) The Exocyst is a multiprotein complex required for exocytosis in *Saccharomyces cerevisiae*. *EMBO J* 15(23):6483–6494.
14. TerBush DR, Novick P (1995) Sec6, Sec8, and Sec15 are components of a multisubunit complex which localizes to small bud tips in *Saccharomyces cerevisiae*. *J Cell Biol* 130(2):299–312.
15. Vega IE, Hsu SC (2001) The exocyst complex associates with microtubules to mediate vesicle targeting and neurite outgrowth. *J Neurosci* 21(11):3839–3848.
16. Inoue M, Chang L, Hwang J, Chiang SH, Saltiel AR (2003) The exocyst complex is required for targeting of Glut4 to the plasma membrane by insulin. *Nature* 422(6932):629–633.
17. Thapa N, et al. (2012) Phosphoinositide signaling regulates the exocyst complex and polarized integrin trafficking in directionally migrating cells. *Dev Cell* 22(1):116–130.
18. Zhao Y, et al. (2013) Exo70 generates membrane curvature for morphogenesis and cell migration. *Dev Cell* 26(3):266–278.
19. Zuo X, et al. (2006) Exo70 interacts with the Arp2/3 complex and regulates cell migration. *Nat Cell Biol* 8(12):1383–1388.
20. Prigent M, et al. (2003) ARF6 controls post-endocytic recycling through its downstream exocyst complex effector. *J Cell Biol* 163(5):1111–1121.
21. Fölsch H, Pypaert M, Maday S, Pelletier L, Mellman I (2003) The AP-1A and AP-1B clathrin adaptor complexes define biochemically and functionally distinct membrane domains. *J Cell Biol* 163(2):351–362.
22. Wu S, Mehta SQ, Pichaud F, Bellen HJ, Quiocho FA (2005) Sec15 interacts with Rab11 via a novel domain and affects Rab11 localization *in vivo*. *Nat Struct Mol Biol* 12(10):879–885.
23. Oztan A, et al. (2007) Exocyst requirement for endocytic traffic directed toward the apical and basolateral poles of polarized MDCK cells. *Mol Biol Cell* 18(10):3978–3992.
24. Babbey CM, Bacallao RL, Dunn KW (2010) Rab10 associates with primary cilia and the exocyst complex in renal epithelial cells. *Am J Physiol Renal Physiol* 299(3):F495–F506.
25. EauClaire S, Guo W (2003) Conservation and specialization. The role of the exocyst in neuronal exocytosis. *Neuron* 37(3):369–370.
26. Friedrich GA, Hildebrand JD, Soriano P (1997) The secretory protein Sec8 is required for paraxial mesoderm formation in the mouse. *Dev Biol* 192(2):364–374.
27. Murthy M, Garza D, Scheller RH, Schwarz TL (2003) Mutations in the exocyst component Sec5 disrupt neuronal membrane traffic, but neurotransmitter release persists. *Neuron* 37(3):433–447.
28. Zhang L, et al. (2009) *Sec-10* knockout increases the neuroactive-drug responses without affecting function of the postsynaptic ionotropic receptors in neuromuscular junctions. *Prog Biochem Biophys* 36(4):410–416.
29. Hunt-Newbury R, et al. (2007) High-throughput in vivo analysis of gene expression in *Caenorhabditis elegans*. *PLoS Biol* 5(9):e237.
30. Jiu Y, Jin C, Liu Y, Holmberg CI, Jäntti J (2012) Exocyst subunits Exo70 and Exo84 cooperate with small GTPases to regulate behavior and endocytic trafficking in *C. elegans*. *PLoS ONE* 7(2):e32077.
31. Clokey GV, Jacobson LA (1986) The autofluorescent "lipofuscin granules" in the intestinal cells of *Caenorhabditis elegans* are secondary lysosomes. *Mech Ageing Dev* 35(1):79–94.
32. Hermann GJ, et al. (2005) Genetic analysis of lysosomal trafficking in *Caenorhabditis elegans*. *Mol Biol Cell* 16(7):3273–3288.
33. Grant BD, Caplan S (2008) Mechanisms of EHD/RME-1 protein function in endocytic transport. *Traffic* 9(12):2043–2052.
34. Naslavsky N, Weigert R, Donaldson JG (2003) Convergence of non-clathrin- and clathrin-derived endosomes involves Arf6 inactivation and changes in phosphoinositides. *Mol Biol Cell* 14(2):417–431.
35. Chen B, et al. (2010) Endocytic sorting and recycling require membrane phosphatidylserine asymmetry maintained by TAT-1/CHAT-1. *PLoS Genet* 6(12):e1001235.
36. Rolls MM, Hall DH, Victor M, Stelzer EH, Rapoport TA (2002) Targeting of rough endoplasmic reticulum membrane proteins and ribosomes in invertebrate neurons. *Mol Biol Cell* 13(5):1778–1791.
37. Li X, et al. (2013) Inactivation of *Caenorhabditis elegans* aminopeptidase DNPP-1 restores endocytic sorting and recycling in tat-1 mutants. *Mol Biol Cell* 24(8):1163–1175.
38. Shi A, et al. (2012) RAB-10-GTPase-mediated regulation of endosomal phosphatidylinositol-4,5-bisphosphate. *Proc Natl Acad Sci USA* 109(35):E2306–E2315.
39. Naslavsky N, Weigert R, Donaldson JG (2004) Characterization of a nonclathrin endocytic pathway: Membrane cargo and lipid requirements. *Mol Biol Cell* 15(8):3542–3552.
40. Howes MT, et al. (2010) Clathrin-independent carriers form a high capacity endocytic sorting system at the leading edge of migrating cells. *J Cell Biol* 190(4):675–691.
41. Gleason RJ, Akintobi AM, Grant BD, Padgett RW (2014) BMP signaling requires retromer-dependent recycling of the type I receptor. *Proc Natl Acad Sci USA* 111(7):2578–2583.
42. Pan CL, et al. (2008) *C. elegans* AP-2 and retromer control Wnt signaling by regulating mig-14/Wntless. *Dev Cell* 14(1):132–139.
43. Yang PT, et al. (2008) Wnt signaling requires retromer-dependent recycling of MIG-14/Wntless in Wnt-producing cells. *Dev Cell* 14(1):140–147.
44. Shi A, et al. (2009) Regulation of endosomal clathrin and retromer-mediated endosome to Golgi retrograde transport by the J-domain protein RME-8. *EMBO J* 28(21):3290–3302.
45. Pompey SN, Michaely P, Luby-Phelps K (2013) Quantitative fluorescence co-localization to study protein-receptor complexes. *Methods Mol Biol* 1008:439–453.
46. Guo W, Roth D, Walch-Solimena C, Novick P (1999) The exocyst is an effector for Sec4p, targeting secretory vesicles to sites of exocytosis. *EMBO J* 18(4):1071–1080.
47. Anitei M, Hoflack B (2012) Bridging membrane and cytoskeleton dynamics in the secretory and endocytic pathways. *Nat Cell Biol* 14(1):11–19.
48. Loubéry S, et al. (2008) Different microtubule motors move early and late endocytic compartments. *Traffic* 9(4):492–509.
49. Traer CJ, et al. (2007) SNX4 coordinates endosomal sorting of TfnR with dynein-mediated transport into the endocytic recycling compartment. *Nat Cell Biol* 9(12):1370–1380.
50. Derivery E, et al. (2009) The Arp2/3 activator WASH controls the fission of endosomes through a large multiprotein complex. *Dev Cell* 17(5):712–723.
51. Allaire PD, et al. (2010) The Connecdenn DENN domain: A GEF for Rab35 mediating cargo-specific exit from early endosomes. *Mol Cell* 37(3):370–382.
52. English AR, Voeltz GK (2013) Rab10 GTPase regulates ER dynamics and morphology. *Nat Cell Biol* 15(2):169–178.
53. Sano H, et al. (2007) Rab10, a target of the AS160 Rab GAP, is required for insulin-stimulated translocation of GLUT4 to the adipocyte plasma membrane. *Cell Metab* 5(4):293–303.
54. Wang T, et al. (2011) Lgl1 activation of rab10 promotes axonal membrane trafficking underlying neuronal polarization. *Dev Cell* 21(3):431–444.
55. He B, Guo W (2009) The exocyst complex in polarized exocytosis. *Curr Opin Cell Biol* 21(4):537–542.
56. Stenmark H (2009) Rab GTPases as coordinators of vesicle traffic. *Nat Rev Mol Cell Biol* 10(8):513–525.
57. Jin Y, et al. (2011) Myosin V transports secretory vesicles via a Rab GTPase cascade and interaction with the exocyst complex. *Dev Cell* 21(6):1156–1170.
58. Liu J, et al. (2012) Exo70 stimulates the Arp2/3 complex for lamellipodia formation and directional cell migration. *Curr Biol* 22(16):1510–1515.
59. Wang S, Hsu SC (2006) The molecular mechanisms of the mammalian exocyst complex in exocytosis. *Biochem Soc Trans* 34(Pt 5):687–690.
60. Heider MR, Munson M (2012) Exorcising the exocyst complex. *Traffic* 13(7):898–907.
61. Brenner S (1974) The genetics of *Caenorhabditis elegans*. *Genetics* 77(1):71–94.